Study of the water sorption and barrier performances of potato starch nano-biocomposites based on halloysite nanotubes

Nadège Follain, Jiawei Ren, Eric Pollet, Luc Avérous

Study of the water sorption and barrier performances of potato starch nano-biocomposites based on halloysite nanotubes

Nadège Follain[1*], Jiawei Ren[2], Eric Pollet[2], Luc Avérous[2]

[1] Normandie Univ, UNIROUEN Normandie, INSA Rouen, CNRS, PBS, 76000 Rouen, France

[2] BioTeam/ICPEES-ECPM, UMR CNRS 7515, Université de Strasbourg, 25 rue Becquerel, 67087 Strasbourg Cedex 2, France

(*) Corresponding Author: Dr. Nadège Follain. Email: nadege.follain@univ-rouen.fr Phone: +33 2 35 14 66 98

Abstract

The barrier performances, in terms of water vapor sorption properties, gas and water barrier performances were analyzed on different starch-based nano-biocomposites. These multiphase systems were elaborated by melt blending starch and halloysite nanotubes at different contents with different plasticizers (glycerol, sorbitol and a mix of both polyols). The influence of the composition was investigated onto the structure, morphology, water sorption and barrier performances. As recently reported, halloysite nanoclay is a promising clay to enhance the properties of plasticized starch matrix. The barrier performances of nanofilled starch-based films were examined through gas and water permeabilities, diffusivity and water affinity. Glycerol-plasticized starch films give fine and more homogeneous nanofiller dispersion with good interfacial interactions, compared to sorbitol ones (alone or mixed), due to stronger and more stable hydrogen bonds. Tortuosity effects linked to the halloysite nanotubes were evidenced by gas transfer analysis, and exacerbated by the good interactions at interfaces and the resulting good filler dispersion. The influence of morphology and interfacial interactions towards water affinity was highlighted by moisture barrier properties. This was a key factor on the reduction of water diffusion and uptake with nanoclay content. A preferential water transfer was observed as a function of a plasticizer type in relation with the phenomenon of water plasticization in the nanocomposite systems.

Keywords: Potato starch, barrier properties, nano-biocomposite, halloysite, water sorption.

1. Introduction

In the two last decades, the development of environmentally friendly materials has attracted a great interest for researchers and industry. To replace non-degradable fossil-based plastics by renewable-based polymers generally extracted from the biomass is now a crucial trend because of the increasing awareness about the depletion of fossil resources and environmental protection. Starch appears as one of the most promising biodegradable and biobased polymers owing to inherent biodegradability, annual availability, abundance and low cost as well as renewability (Avérous, 2004; He et al., 2012). The use of starchy matrixes to develop hybrid nanomaterials composed of nano-fillers is an innovative and trendy process with a green chemistry approach to obtain performing materials (Alexandre & Dubois, 2000). In this way, native starch can be transformed into thermoplastic-like materials under destructuring and plasticizing conditions using extrusion process or batch mixer (Swanson et al., 1993; Chivrac et al., 2010a; Schmitt et al., 2012; Ren et al., 2018). Starch films can be prepared from different renewable sources with a variability of the properties. For instance, potato starch is found to present higher mechanical properties than most of other sources with a low protein content (He et al., 2012). Starch materials present strong limitations such as low degradation temperature and high brittleness which can be overcome using appropriate plasticizers to improve flexibility and processability of materials. The most commonly used plasticizers are water and polyols such as glycerol or sorbitol (Lourdin et al., 1997; Gaudin et al., 2000; Chivrac et al., 2010a and 2010c, Zeppa et al., 2009). These two types of plasticizers are usually combined with starch: (i) the volatile plasticizer, mainly water, also acts as a destructuring agent, and (ii) the non-volatile plasticizer such as polyols (sorbitol, glycerol and a mixture of both polyols) is added to improve flexibility and processability. During the thermomechanical process, native starch organization is destructured into a molten continuous material to obtain thermoplastic starch by adding these different plasticizers. Thermoplastic starch materials show great potential for short-term applications such as agricultural mulch films and some packaging (He et al., 2012; Xie et al., 2013; Wu et al., 2019).

One way to improve starch properties in terms of notably mechanical and thermal properties and especially barrier properties is to incorporate nano-sized fillers (Wu et al., 2019; Bertolino et al., 2020) while preserving biodegradability and biocompatibility of starch

matrix (Avérous, & Pollet, 2012) without generating toxic byproducts. The dispersed nanofillers are viewed as impermeable entities, increasing tortuous diffusion pathways for small diffusing molecules (Gorrasi et al., 2003), such as water and gas species. Then, gas and water barrier performances of a film can be significantly improved (Alexandre, & Dubois, 2000; Zeppa et al., 2009; Chivrac et al., 2010; Xie et al., 2013; Cheviron et al., 2016; Follain et al., 2013; Follain et al., 2016). Main used nanofillers are layered silicates such as montmorillonite (MMT) (Chivrac et al., 2010a; Xie et al, 2013, Wu et al., 2019). According the level of MMT organomodification, the layered silicates can be intercalated by polysaccharides chains and even slightly exfoliated. Some authors have shown phases segregation within the plasticized starch matrix as a function of plasticizers content with glycerol-enriched phases and carbohydrate-MMT enriched microphases (Chivrac et al., 2010a). Some studies on intercalated starch systems exhibited reverse results (Chivrac et al., 2010a; Cheviron et al., 2015) even in the case of cationic starch as MMT organo-modifier to favor clay exfoliation. The tendency of nanofillers to form agglomerates is not fully solved even in the case of using the most convenient preparation method, such as melt mixing (Bertolino et al., 2020). In addition, the influence of plasticizers content on the clay intercalation/exfoliation process and on the resulting materials properties has been highlighted: reduced plasticization effect on the starch phase, reversion in mechanical properties or decline in the moisture property (Xie et al, 2013). It seems that a competition between starch-glycerol interactions with the interactions with the nanofiller surfaces took place depending on the plasticizer content.

Recently, halloysite nanotubes, multi-wall kaolinite nanotubes, presenting a large aspect ratio, high functionality and high mechanical properties have been presented as an interesting alternative to silicates. In this case, the hydroxyl groups are mainly present on the internal surface while siloxane groups are located at the external surfaces of nanotubes with silanols/aluminols present mainly at the edges of the platelets (Wu et al., 2019). Due to their stable tubular morphology, unique micro/nanostructure, the halloysite nanotubes can be dispersed into single particles easily and the lumen diameter fits well to macromolecule and protein average diameters (Wu et al., 2019; Ren et al, 2018), even high content (Bertolino et al., 2020) and therefore reduces the extent of filler-filler aggregation in the matrix compared to MMT for instance. Several halloysites nanotubes and polysaccharides systems have been

studied (Pasbakhsh et al., 2018), based on starch (He et al., 2012; Ren et al., 2018), pectin (Makaremi et al., 2017), cellulose (Nechyporchuk et al., 2016) or alginate (Wang et al., 2019).

However, the investigation of barrier properties is still rarely reported for these systems, and even less on plasticized nano-biocomposites. The "morphology-barrier properties" relationships are rarely evaluated on such systems. Besides, among the rare published studies dealing with gas and/or water transport properties for plasticized starch nano-biocomposites, none clearly detailed approach of transport properties in which filler tortuosity effects, water diffusivity with plasticization effect and water hydration properties are associated with morphology was reported.

This paper complements and substantially extends previous reported studies on the elaboration of nano-biocomposites based on clay nanofillers (Chivrac et al., 2010a) and on halloysite nanotubes (Ren at al., 2018) to understand the transport mechanisms as a function of plasticizer types and filler content. Then, the main objective of this work is to carefully study the gas barrier performances, water sorption characteristics, and water vapor barrier properties of series of nano-biocomposites systems based on thermoplastic potato starch filled with halloysite nanotubes. In order to understand better these systems, variations are brought through the formulation of these multiphase biobased structures.

2. Materials and methods

2.1. Materials

Potato starch (with the following composition: 80% starch, 19.5% moisture, 0.05% proteins and 0.2% ash) from Roquette (Lestrem, France) was used as matrix. The ratio wt%/wt% of amylose and amylopectin was 20%/80%. Glycerol (G) was a 99.5% purity product (Thermo Fisher Scientifc, Illkirch-Graffenstaden, France). Sorbitol (S) with a purity of 98% was kindly supplied by Tereos (Origny-Sainte-Benoite, France). Polysorb® (P) containing 59 wt% glycerol content and 41 wt% sorbitol content was kindly supplied by Roquette (Lestrem, France). The halloysite nanotubes with a diameter of 30-70 nm and a length of 1-3 μm were purchased in Sigma-Aldrich (Lyon, France).

2.2. Nano-biocomposites preparation and stabilization

126 The preparation method was particularly described in a previous paper (Ren et al., 2018).
127 The formulation used in this study contained 54 wt% of native potato starch, 23 wt% of
128 polyol plasticizer and 23 wt% of water. Typically, after a drying overnight at 70°C in a
129 ventilated oven for removal of free water (around 10% of the solids), the dried potato starch
130 was introduced into a Papenmeier turbo-mixer with plasticizers slowly added under mixing
131 at high speed (1700 rpm) for few minutes until a homogeneous mixture was obtained
132 (Chivrac et al., 2010c). Placed in a ventilated oven at 170°C for 40 min, and occasionally
133 stirred, allowing volatilization of the bound water with an exchange by diffusion of the
134 plasticizer molecules towards the starch macromolecules. Such a method allows the
135 preparation of plasticized starch with high plasticizer content without exudation
136 phenomenon, mainly due to the stronger interactions established between the
137 polysaccharide chains and the polyols (Chivrac et al., 2010c). The obtained dry-blend was
138 recovered. In order to obtain the adequate moisture content (i.e. 23 wt%), water was added
139 to the dry-blend after cooling and mixed in the turbo-mixer for few minutes (Chivrac et al.,
140 2010c). Finally, the plasticized starch powder was stored in a polyethylene bag in a
141 refrigerator at 6°C overnight prior to processing.

142 To obtain nano-biocomposites, halloysite nanotubes (3 and 5 wt% relative to the dry-blend
143 (d.b.) weight) were added to the plasticized starch powder by using a counter-rotating
144 internal batch mixer, RheomixOS (Haake Thermo Fisher Scientific, Illkirch-Graffenstaden,
145 France) at 70°C for 20 min with a rotor speed of 150 rpm. After melt processing, the systems
146 were then compression molded (Labtech Engineering Company, Muang, Thailand) at 110°C
147 by applying 18 MPa pressure for 15 min. 200 µm-thick films were finally obtained.

148 Designation of the films is based on G for glycerol, S for sorbitol and P for the mixture. For
149 instance, G0, G3 and G5 is for the glycerol-based systems with 0, 3 and 5 wt. % of halloysite
150 nanotubes, respectively.

151 It has been already shown that stable properties were mainly obtained after around 1 month
152 of ageing at 57% RH (i.e. Relative Humidity) for G-plasticized wheat starch-based films
153 (Chivrac et al., 2010a). In that respect, the 200 µm-thick films were stored at 57% RH at
154 room temperature to ensure stabilized properties. Before each characterization, the film
155 thickness was measured on more than 10 random positions on the film to obtain an average
156 thickness. The average deviation is found to be around 5%.

2.3. Characterizations

2.3.1. Scanning Electron Microscopy (SEM)

Using an operating voltage of 5 kV and ×10,000 magnifications, Scanning Electron Spectroscopy images were performed on cryo-fractured surfaces of the films with a VEGA3 LM scanning electron microscope (TESCAN, Brno, Czech Republic). The samples were mounted on a stub using double-sided adhesive tape and coated with a thin layer of gold (10-20 nm).

2.3.2. X-ray Diffraction (XRD).

X-ray diffraction analysis was carried out on a Bruker AXS D8 Advance (Bruker, Wissembourg, France) using Cu-Kα radiation (λ=0.1542 nm) operating at 50 kV and 40 mA. The scanning region of the diffraction angle (2θ) was from 10° to 50° with a step size of 0.02°.

2.3.3. Gas permeation measurements.

Permeation to carbon dioxide and oxygen (99.9% purity, Air Liquide) were performed at 25°C by means of a lab-built device based on the time-lag barometric determination (Métayer et al., 1999). A preliminary high vacuum desorption was performed on the cell measurement containing the sample. When applying a gas pressure, the quantity of transferred gas through the film was monitored until reaching the stationary state of the permeation process. This is detected by a constant increase of gas pressure by the pressure sensor at the permeation die. The permeability coefficient P was directly determined by Equation 1:

$$P = \frac{J_{st} \cdot L}{\Delta p} \quad \text{(eq. 1)}$$

Where J_{st} is the stationary flux and Δp is the pressure difference between the two faces of the film, L is the film thickness and P is expressed in Barrer (1 Barrer = 10^{-10} $cm^3_{(STP)}$ cm cm^{-2} s^{-1} cm_{Hg}^{-1}).

The measurements were at least duplicated from two different samples per tested film for reproducibility.

The separation performances can be determined from selectivity factor $\alpha_{A/B}$ which is calculated from the ratio of permeability of gas pairs is given by Equation 2 (Prager, & Long, 1951):

$$\boldsymbol{\alpha_{A/B} = \frac{P_A}{P_B}} \quad \text{(eq. 2)}$$

where P_A and P_B are the permeability coefficients of the more and less permeable gas, respectively (Ashley, 1985).

2.3.4. Water permeation measurements.

Water permeation measurements were performed using a lab-built setup (Métayer et al., 1999) composed of a measurement cell, containing two compartments separated by the tested film, enclosed in a chamber thermoregulated at 25 °C. The sensor, a chilled mirror hygrometer (General Eastern Instruments, U.S.A.), was placed in the downstream compartment of the measurement cell. After a long drying step using dry nitrogen gas flow (99.999% purity, Air Liquide), pure water (Milli-Q water system, resistivity 18 MΩ·cm^{-1}) was introduced in the upstream compartment of the measurement cell. The water flux *J*, resulting from the water transfer through the film, was recorded as a function of time in the downstream compartment using the sensor. Once the humidity value was stable, indicating the steady state of the permeation, the permeation measurement was considered as completed. The measurements were repeated twice for each film. The permeability coefficient *P* of the film was deduced from the steady state of the water flux J_{st} by Equation 3:

$$P = \frac{J_{st} \times L}{\Delta a_w} \quad \text{(eq. 3)}$$

where J_{st} is the stationary flux, L is the film thickness and Δa_w is the difference in water activity across the tested film. The P_{H2O} coefficient can be expressed in Barrer or converted in SI unit (with 1 Barrer = 10^{-10} $cm^3_{(STP)}$ cm cm^{-2} s^{-1} cm_{Hg}^{-1} = 3.35×10^{-16} mol m m^{-2} s^{-1} Pa^{-1}).

The water permeation experiments were at least duplicated from two different specimens per tested film for reproducibility.

2.3.5. Water diffusion coefficient

The diffusion coefficient D was deduced from the transient regime of the water flux curves, when plotting the flux J/J_{st} as a function of the reduced time τ $(= D \times t/L^2)$ in dimensionless scales of flux and time. By assuming a Fickian mechanism of diffusion, two diffusion coefficients can be determined at two specific times of the permeation process, that are the inflexion point I ($j_I = J/J_{st} = 0.24$, $\tau_I = 0.091$) and the time-lag point L ($j_L = J/J_{st} = 0.6167$, $\tau_L = 1/6$), as described in a separate paper (Marais et al., 1999). The first coefficient, noted D_I ($D_I = L^2 \times 0.091/\tau_I$), is calculated at a reduced time τ_I corresponding to the inflexion point I of the theoretical flux curve (Marais et al., 1999). The second coefficient, D_L ($D_L = L^2/6.\tau_L$), is calculated at a reduced time τ_L relative to the time-lag point L of the theoretical flux curve (Marais et al., 2000). In the case of D_I is practically equals to D_L, the diffusion coefficient D is assumed to be constant. Nevertheless, the D_I coefficient is generally found to be smaller than the D_L coefficient, which evidences a dependence of the diffusion coefficient with the water concentration, caused by the plasticization effect of water (Follain et al., 2010). This dependence is usually represented by an exponential law with Equation 4:

$$D = D_0 \times e^{\gamma C} \qquad \text{(eq. 4)}$$

where D_0 (in $cm^2.s^{-1}$) is the limit diffusion coefficient, γ (in $cm^3.mmol^{-1}$) is the plasticization coefficient and C (in $mmol.cm^{-3}$) is the local concentration of sorbed water. The precision on the diffusion coefficients was around 5%.

2.3.6. Water vapor sorption kinetic.

The water vapor sorption kinetic measurements were performed using an electronic microbalance Cahn D200 enclosed in a gravimetric dynamic vapor sorption analyzer (Surface Measurement Systems, Ltd., London, UK), as previously described (Follain et al., 2013; Follain et al., 2016). The measurement temperature was set at 25.0 (± 0.1) °C. The water activity a_w (0 – 0.90 by step of 0.1) was adjusted by mixing dry and moisture-saturated nitrogen flowing (N_2 gas, 99.999 % of purity, Air Liquide) using electronic mass flow controllers. Approximately 8 mg of polymer film (diameter of 8 mm) was initially dried until no further change in dry mass was measured and then submitted to a hydration cycle by exposure to selected water vapor pressures. The film mass evolution was recorded with time as a function of water activity and the sorption kinetics was followed step by step until the

weight at equilibrium was reached. Water vapor sorption isotherms were determined from the dry mass and the mass at equilibrium state for each water activity. Duplicates were performed for each film for reproductibility. The water mass gain was determined by Equation 5:

$$C_{eq}(\%) = \frac{M_{eq} - M_0}{M_0} \times 100 \quad \text{(eq. 5)}$$

Where M_0 and M_{eq} are the dry sample mass and the sample mass at equilibrium state, respectively.

2.3.7. Water vapor kinetic analysis.

Sorption kinetic data were analyzed in terms of water diffusivity by using the analytical solutions of Fick's law by taking into account the usual boundary conditions for gas and vapor sorption measurements (Follain et al., 2010). In the present work, different parameters must be taken into account such as i) the films were treated as dense and homogeneous materials for which diameter to half thickness ratio is higher than 80 meaning that the diffusion from the edges of the film can be neglected, ii) the transport phenomenon is governed by a solution-diffusion mechanism, iii) the mass transfer is in the perpendicular direction to the plane sheet with instantaneous interfacial sorption equilibrium (Crank, 1967), and iv) the water concentration gradient is only along the x-axis. The diffusivity is a measure of the ability of water molecules to move by random molecular motions through the polymer film. Assuming a constant diffusion coefficient, the total mass sorption of the water molecules $\frac{M(t)}{M_{eq}}$ can be described by Equation 6 (Follain et al. 2010):

$$\frac{M(t)}{M_{eq}} = 1 - \frac{8}{\pi^2} . \sum_{n=0}^{\infty} \frac{1}{(2n+1)^2} \exp\left(-\frac{\mathrm{D}\,(2n+1)^2 . \pi^2 . \mathrm{t}}{L^2}\right) \quad \text{(eq. 6)}$$

Where $M(t)$ and M_{eq} are the masses of sorbed water at time *t* and at equilibrium state, respectively, L is the film thickness and D is the diffusion coefficient.

For each water activity, the diffusion coefficient D (expressed in $cm^2.s^{-1}$) was calculated for the short time (up to 50% of M_{eq}, i.e. when $\frac{M(t)}{M_{eq}} < 0{,}5$) according to Equation 7:

$$\frac{M(t)}{M_{eq}} \approx \frac{4}{L} . \sqrt{\frac{D}{\pi}} . \sqrt{t} \qquad \text{With} \quad D = \frac{k . \pi \cdot L^2}{16} \quad \text{(eq. 7)}$$

Where k_1 stands for the coefficient for the short time.

The precision on the diffusion coefficients was estimated to be lower than 5%.

3. Results and discussion

3.1. Morphological analysis and crystallinity aspect

Properties of nanocomposite films are highly dependent on their microstructures. For this purpose, the evaluation of their morphology, and "starch-plasticizers-nanoclay" interactions have to be determined in order to correlate these parameters with the barrier properties of plasticized starch films. Most of the different parameters for the starch/halloysite nanotubes bio-nanocomposites have been fully reported in a previous publication, notably in terms of morphology, thermal and mechanical properties (Ren at al., 2018). In that case, we proposed to briefly report the main characteristics of these films to highlight and explain water vapor sorption behavior and transport properties exclusively evaluated in the present work.

The crystallinity of films was found to be around 10% on agreement with literature on starch-based systems taking into account the formulation (Van Soest et al., 1996a; Chivrac et al., 2010a). With the incorporation of halloysite nanotubes, no significant variations of the matrix crystallinity were found. Nanocomposites displayed similar crystalline structures as the neat starchy films (Chivrac et al. 2010a; Ren et al., 2018). Then, the degree of crystallinity being constant, one can infer that the evolutions in water sorption and transport properties is only correlate to the nano-biocomposite microstructure (nanoclay dispersion, quality of interfacial interactions, presence of voids, etc.).

Briefly, some trends concerning the morphology and thermal properties of the plasticized starch/halloysite nanotubes bio-nanocomposites are reported thereafter, based on published Ren's work (Ren et al., 2018). In absence of halloysite nanoclay, the plasticizer effect on the microstructure of starch-based films was evaluated. For the G-based starch film, uniform morphology was obtained with a completely disrupted starch structure because any starch granule layers were observed after the thermo-mechanical process applied to starch powder (Ren et al., 2018). But, the presence of some voids was noted within the film showing a discontinuous morphology. Contrary, more uniform and continuous morphologies, without remaining starch granules, were obtained for the S-based

297 and P-based starch films. From these observations, one can infer a better plasticizer
298 dispersion owing to the greater shear force during the S addition (Ren et al., 2018).

299 The morphology was altered with the incorporation of halloysite nanoclay into the
300 plasticized starch. For the G-based starch films, the morphology became continuous with a
301 homogenous dispersion of individual nanotubes. The absence of interfacial voiding from
302 SEM images has indicated a good nanoclay-matrix interfacial interaction (Ren et al., 2018).
303 By contrast, large nanoclay aggregates were present in the S- and P-based starch films (Ren
304 et al., 2018) with interfacial voiding which indicates a poor interfacial interaction. For the
305 starch films plasticized by the polyols mixture, very small aggregates were viewed with a
306 large proportion of randomly dispersed individual nanotubes. From these findings, one can
307 say that the presence of G in the polyols mixture tends to favor the dispersion of nanotubes
308 within the starchy matrix (Ren et al., 2018).

309 To investigate the interactions between plasticized starch and halloysite nanoclay, ATR-FTIR
310 analyses were carried out (Ren et al., 2018). The vibrational stretching band related to the
311 free, inter- and intra-molecular bound hydroxyl groups of starch was observed between
312 3000 and 3600 cm^{-1}. Concerning starch plasticization, an absorption band of O-H stretching
313 was shifted to lower wavenumbers reflecting strong and stable hydrogen bonds formed
314 between plasticizers and the starch macromolecules. For the glycerol plasticized starch
315 nano-biocomposites (Ren et al., 2018), the O-H stretching peak of inner-surface hydroxyl
316 groups (at 3693 cm^{-1}) was shifted to lower wavenumber, that is 3691 cm^{-1}, as already
317 observed by Schmitt et al. (Schmitt et al., 2012). The authors have attributed this shift to the
318 formation of interactions between the inner-surface hydroxyl groups of halloysite nanoclay
319 and the C-O-C groups of starch and/or glycerol. On the contrary, in presence of sorbitol,
320 alone or in mixture with glycerol, as plasticizer of starch, this peak was shifted to a higher
321 wavenumber, 3696 and 3694 cm^{-1} i.e. for S5 and P5, respectively (Ren et al, 2018). In that
322 case, a decrease in intermolecular interactions between the inner-surface hydroxyl groups of
323 halloysite and the C-O-C groups of starch and/or plasticizers was considered. Ren et al. (Ren
324 et al., 2018) have inferred that stronger and more stable hydrogen bonds are formed with
325 glycerol compared to the case with sorbitol, alone or in mixture with glycerol. This
326 phenomenon can explain the better dispersion of halloysite nanoclay in glycerol-based
327 starch films.

To summarize the XRD analyses obtained for these systems (Ren et al., 2018), the characteristic diffraction peaks of the E_H-type and V_H-type structures of starch after plasticization with G, due to the amylopectin recrystallization and amylose crystallization, respectively, were shown (van Soest et al., 1996b). Similar pattern to the G-based starch film was obtained for the P-based starch film. Additional small peaks at around 12.0 and 18.8° were assigned to the well-known storage-induced crystallization of S (Talja et al., 2007) and were only viewed for S-based starch film (Ren et al., 2018). For the nanocomposite films, the characteristic patterns of the plasticized starch matrix were also observed with those of the filler, ensuring that halloysite nanoclay are well dispersed in the matrix. In addition, some specific characteristics were also be noted. For the G-based starch films, a new peak at 28.5° was obtained due to the amylopectin crystallization at the filler-starch interfacial areas by establishment of strong filler-starch hydrogen bonds (Ren et al., 2018), as already reported for starch/tunicin cellulose whiskers (Anglès et al., 2000) and starch/sepiolite filler nanocomposites (Chivrac et al., 2010b). This finding is also in agreement with studies relating to PP/halloysite nanocomposites (Liu et al., 2009) or PVDF/halloysite nanocomposites (Tang et al., 2013). This new peak was partly observed for the S-based starch nanocomposites due to the filler aggregation in the S-based starch interfering with the amylopectin crystallization. For the P-based starch nanocomposites, the presence of G in the plasticizer mixture has favored the amylopectin crystallization due to a higher halloysite dispersion in the starch matrix. Hence, this new peak was more visible. Similar observations were reported for plasticized wheat starch-based films containing organo-modified MMT with cationic starch (organo-modifier) as a function of polyol plasticizer type and nanofiller content (Chivrac et al., 2010c) One can infer that the good nanofiller-starch interfacial interactions and the good nanofiller dispersion developed within the G-based nanocomposite films can be related to the strong polar interactions between the hydroxyl (OH) groups of the starch chains, of the G, and of the halloysite nanotubes.

3.2. **Tortuosity effect**

Carbon dioxide and oxygen were selected as probes to investigate gas barrier properties of films and to evaluate the nanofiller/starch interfaces. These gases present a high capacity of diffusion through a substrate due to low Van der Waals molar volumes (42.67 and 31.83 cm^3/mol for O_2 and CO_2, respectively) (Baker, & Wijmans, 1994). The gas permeation curves

for the nanocomposites were fitted by the linear Henry's law which is an indication that the diffusion coefficient D is constant during measurements so that the P=D.S equation is effective. The permeability coefficients are summarized in Figure 1. The obtained values are in the same order than those previously reported in the literature (Gaudin et al., 2000; Cheviron et al., 2016). However, a direct comparison with the values of the literature is not relevant because experimental conditions and environment can modify the gas transfer, such as (i) the process (cast films vs. extruded films, (ii) the formulation with the botanical origin of the starch, the type and the content of plasticizers, (iii) the storage conditions of films, and (iiii) the permeation device used as well as the experimental conditions applied (temperature, gas pressure).

From a general point of view, the permeability ranking is found to be $P_{CO2}>P_{O2}$, irrespective of the tested films, which is consistent with the works of Van Krevelen (Van Krevelen, 1997). This directly results from the nature and size of gas species. For CO_2 and O_2 gases, the permeability is mainly governed by the gas condensability, i.e. by the gas solubility, which is dependent on the boiling and critical temperatures of diffusing species. In the present case, CO_2 gas presents a lower Van der Waals molar volume (31.83 cm^3/mol (Baker, & Wijmans, 1994)) and a higher critical temperature (31.2°C) than O_2 gas, which explains the greater CO_2 permeability for the films.

Regarding the unfilled plasticized films, the G-plasticized starch film has displayed higher permeability coefficients than the P-plasticized starch film and the S-plasticized starch film, respectively. Based on the SEM images (Ren et al., 2018) and the literature on G-plasticized starch matrixes, the discontinuous morphology for the G-plasticized starch film has favored the gas molecules transfer, explaining the highest gas permeability. It was already mentioned in the literature that the relatively high plasticizer content (23 wt% G) induces a phase separation, with carbohydrate rich and plasticizer rich phases (Chivrac et al., 2010a). Accordingly, a preferential diffusion pathway for gas molecules was created in this discontinuous morphology. Contrariwise, the continuous and uniform morphologies of the P-plasticized starch film and the S-plasticized starch film explain the low gas permeabilities. The gas permeation measurements are generally a way to evidence the tortuosity effects exerted by crystalline phase of matrix or by inorganic fillers when polymeric and/or nanocomposite films are tested. In the present case, i.e. without filler, the lowest

permeability for the S-plasticized starch film is an indication of higher tortuosity effects than the P-plasticized starch film. This can be likely related to the storage-induced S crystallization, as shown by the XRD patterns (Ren et al., 2018), that brings some additional crystallinity.

Regarding the incorporation of halloysite nanotubes in the plasticized starch matrix, a reduction in gas permeability coefficient is clearly obtained as the filler content increases, whatever the gas tested. Likewise, a reduction in oxygen permeability, tested at different relative humidities, was also reported for plasticized potato starch films containing few percent of raw MMT (Masclaux et al., 2010). This attests for effects of tortuosity resulting from the presence of the nanofiller. Usually, the nanofillers are considered as common obstacles to the diffusion species through materials generating tortuosity effects. In the present work, these effects seem to be exacerbated by the quality of nanofiller-starch interfacial interactions as well as by the nanofiller dispersion in the starch matrix. In fact, one can see that the reduction in gas permeability is greater for G-plasticized series. This phenomenon is linked to the better dispersion of halloysite nanoclay in starch matrix due to intermolecular interactions between halloysite nanotubes and starch and / or glycerol without nanoclay aggregates, as revealed from SEM images, ATR-FTIR analyses and XRD analyses (Ren et al., 2018). Longer diffusion pathways likely due to greater tortuosity effects of the nanofiller can explain this trend. For the two other series, the presence of aggregates and the weaker quality of interfacial interactions, leading to some voids (free spaces) between nanoclay aggregates and starch matrix, induce a lower reduction in gas permeability. Only, an increase of permeability coefficient of the two gases is obtained for the S5 nanocomposite film. The presence of large nanofiller aggregates initiating free volume within the film has consequently improved the gas diffusion with specific diffusion pathways.

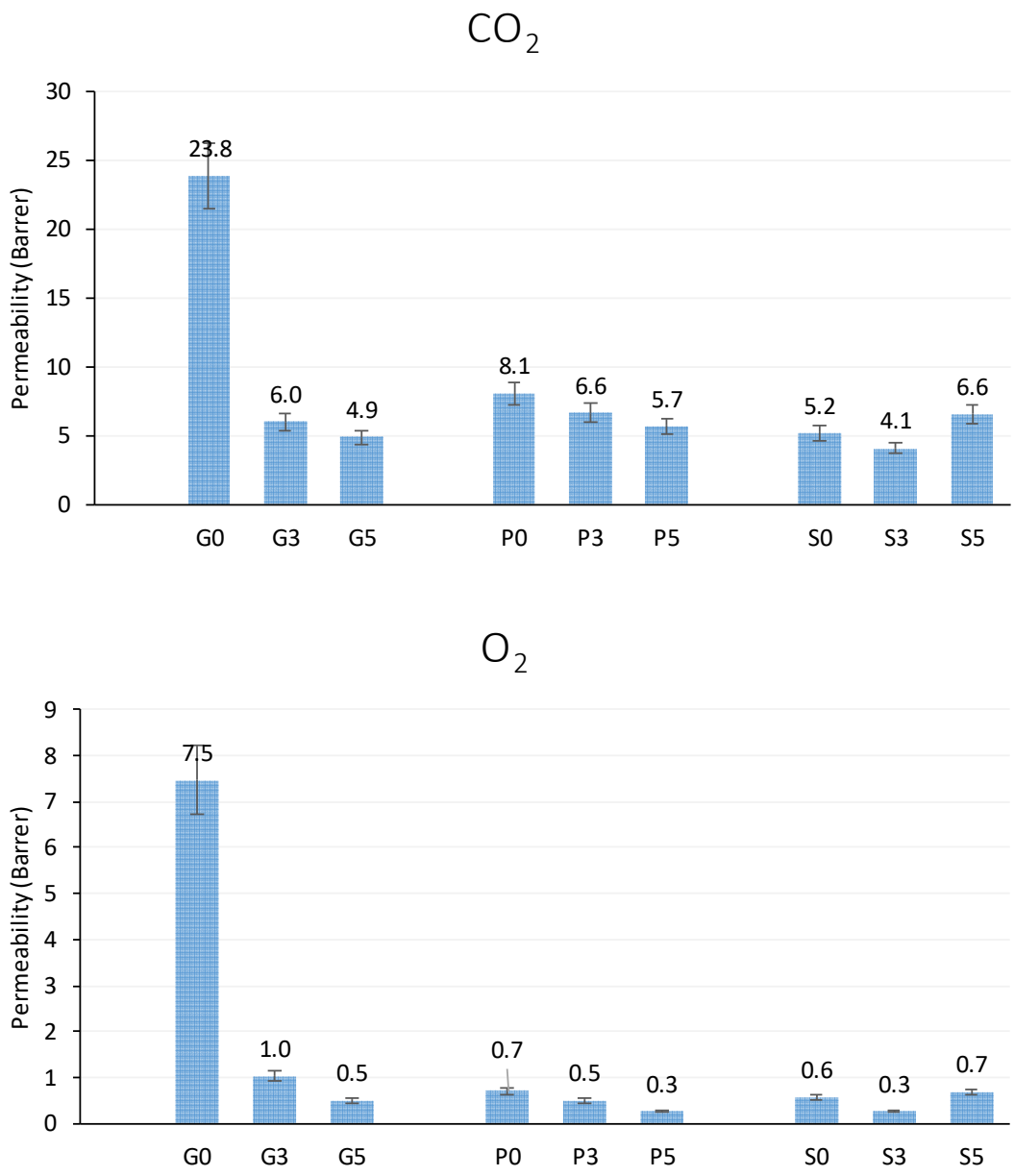

Figure 1. Carbon dioxide (top) and oxygen (bottom) permeability coefficients for the plasticized starch nano-biocomposites based on G, P and S plasticizer systems with different nanofiller contents (0, 3 and 5 wt%). The average variation of coefficients is found to be 10%.

The gas permeability data can be correlated with the selectivity factor α, which was calculated from the ratio of the permeabilities of gas pairs (P_{CO2}/P_{O2}). The selectivity factor allows highlighting the ability of a material to separate gas mixture. It is usually assumed that a factor higher than 10 outlines the gas selectivity of the material with a preferential transfer of the more permeable gas against to the other one. The selectivity factors for the three series of plasticized starch nanocomposites are summarized in Table 1. The main result is

that the selectivity calculated for the G-based starch series is beneath the two other ones, and the series plasticized with the P mixture presents the highest selectivity factors. According to the Robeson's statements (Robeson, 2008), the selectivity factors calculated for the latter series are in the same range as those of usual polymer films. Then, as usually observed, the more selective the film, the lower the permeability. However, the obtained factors are not high (>20) so that the series of films can be viewed as gas high-barrier films with an interesting permselectivity.

For the G-based starch nanocomposites, the selectivity factor continually increases as the filler content increases. This is an indication that the nanocomposites are more gas selective with halloysite nanotubes. A similar observation can be shown with the P-based starch films series at a higher extent. Unlike, the S-based starch films display a reverse effect. At 3 wt% of halloysite filler, the selectivity factor increases whereas the factor decreases at higher content, i.e. 5 wt%. This finding can be related to the specific microstructure of the three films series (Figures S1 and S2 in SI). The S-based starch films exhibit the worst interfacial filler-starch interactions with the presence of large aggregates as the filler content increases. Thus, the diffusion pathways occur in these lesser cohesive areas facilitating the gas diffusion.

Selectivity $\alpha=P_{CO2}/P_{O2}$ at the three nanofiller content (wt%)	**G-plasticized films**	**P-plasticized films**	**S-plasticized films**
0	3.2	11.3	9.2
3	5.8	13.1	15.3
5	9.6	21.2	9.6

Table 1. Selectivity (P_{CO2}/P_{O2}) for the plasticized nano-biocomposites with different nanofiller contents (0, 3 and 5 wt%) and plasticizer systems (P, G and S). The average variation of coefficients is found to be 10%.

3.3. Water-material interactions

Since water molecules strongly interact with polysaccharide chains, water behavior was also investigated. The amount of water molecules crossing the processed films was determined by permeation kinetics measurements. The humidity content was also measured downstream of the film. From permeation kinetics, the water permeability and the water

diffusion coefficients characterizing the overall water barrier properties are determined from the steady state and the transient regime of permeation process, respectively. These values allow highlighting the nanofiller-starch macromolecular systems interfacial interactions.

3.3.1. Water permeability versus filler content

Water permeability coefficients for the three series of films are presented in Figure 2. The obtained values are in good agreement with those reported in the literature for plasticized films prepared from corn starch (Tang et al., 2008) or from potato starch (Rindlav-Westling et al., 1998; Cheviron et al., 2015).

For the unfilled starch films, the films plasticized with G or P mixture present the highest permeability coefficients. This result can be related to the high hydrophilicity of G. An intimate affinity between permeated water molecules and plasticized starchy materials is also observed, as regularly claimed by other authors in the literature for plasticized natural films. The lower permeability coefficient measured for the film plasticized with S can be explained by the lower hydrophilic character of S and by the obtaining of a brittle film. In fact, some of us in a previous paper have shown that a S-plasticized starch film had the highest Young's modulus, ten times higher than a G-plasticized starch film, the lower strain at break values with a reinforcement effect with the addition of halloysite nanotubes (Ren et al., 2018). Both results can be in line with the conventional S crystallization during storage which could embrittle starch materials

Regarding the halloysite nanotubes incorporation, an unexpected increase of water permeability coefficients was obtained for the three series of films, compared to the values of the unfilled films. Although inconsistent results were mentioned in the literature (water permeability reduction or water permeability increase (Chivrac et al., 2010a)), the permeability change is in accordance with the diffusion coefficient change, as discussed later. This reflects that tortuosity effects exerted by nanofiller with tube-like structure were not sufficient enough for reducing the water permeability owing to the water affinity, and likely due to morphology. The hydrophilic functions on the nanofiller surface have also driven the increase in water permeability coefficient, as classically reported for hydrophilic nanofillers (Chivrac et al., 2010a)

As the nanofiller content increases, two different trends are observed: (i) an increase of permeability for the S5 nanocomposite and (ii) a reduction of permeability for the G5 and P5 nanocomposites. These reverse behaviors could be likely linked to the microstructure of the corresponding films. For the S5 film, the combination of poor interfacial interactions and large nanofiller aggregates has contributed to create free volumes along the interfacial areas and domains free of fillers accessible to water molecules, leading to formation of preferential diffusing pathways. This was supported by SEM observations and highlighted from gas permeation measurements. For the two latter films, the good filler-starch interfacial interactions have hampered the water transfer through film, in association with tortuosity effects induced by the fine dispersion of halloysite nanotubes. In that case, longer and tortuous diffusion pathways are obtained (Bharadwaj, 2001; Gorrasi et al., 2003). Similar observations have been made as a function of nanofiller dispersion state for polymer/MMT nanocomposite films (Gorrasi et al., 2003; Follain et al., 2016) or for plasticized wheat starch films (Chivrac et al., 2010a). In this latter case, an increase in water vapor permeability is measured as MMT content increase, even in the case of well exfoliated nanoclay within the plasticized starch matrix. According to these authors, it seems that preferential water diffusion pathways were created in domains where layered silicates were almost totally absent, namely the G rich-phases, due to the phase segregation within the G-plasticized starch matrix. In the present work, the continuous and homogeneous morphology was rather obtained in presence of halloysite nanotubes with a fine dispersion of halloysite nanotubes which tends to favor a water permeability decrease.

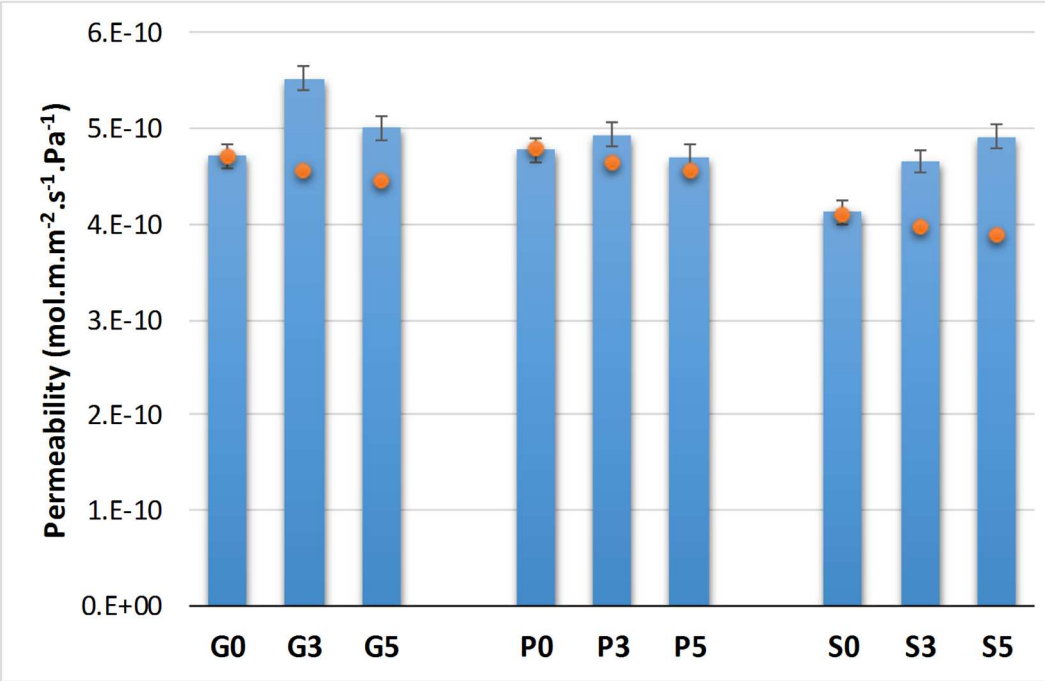

Figure 2. Water permeability of the nano-biocomposites with different nanofiller contents (0, 3 and 5 wt%) and plasticizer systems (G, P and S).

The circle symbol is used to mark a theoretical water permeability obtained from a simple additivity law (e.g., 97% of matrix + 3% of impermeable filler for the starch-based nanocomposite with 3 wt% of halloysite).

To evidence tortuosity effects of nanofiller, assuming that nanofillers are impermeable entities, one can calculate a theoretical permeability coefficient using a simple additivity law. The circle symbols in Figure 2 represent these theoretical values. Two cases are possible if the values diverge:

i) the calculated values are higher than the experimental values meaning that the film is more barrier to water due to higher tortuosity effect,

ii) the calculated values are lower than the experimental values meaning that the film is more permeable to water. In this case, this divergence shows the affinity of the permeated molecules with the films.

One can note that the experimental values are always higher for the three series of films. This divergence thus highlights a certain affinity with water molecules, directly linked in the present case to the hydrophilic contribution of nanofiller. Thus, permeating water molecules act as a plasticizing agent. The creation of percolating diffusion pathways during water

transfer appears also to have been favored according to the morphology and filler dispersion state. The divergence between theoretical and experimental permeability coefficients is however not so high, meaning that tortuosity effects, evidenced from gas permeation measurements, are counterbalanced by changes in free volume with the influx of additional water molecules during the water permeation and by the quality of the filler-plasticized starch interfacial interactions.

Moreover, irrespective of changes in permeability coefficients, one can note that water molecules have been more readily absorbed into the films surface and can easily penetrated through the film structure as a plasticizer, if we consider the profiles of the permeation curves (Figure 3). The water permeation kinetics were commonly corrected with reduced time (tL^{-2}) to overcome the film thickness effect (Figure 3). The water permeation curves can be usually divided into three different domains:

i) at starting measurement, JL is equal to 0 indicating that no water diffused through the film;
ii) with the water diffusion, the water flux is increased corresponding to the transient regime of permeation from which the diffusion coefficient is determined, and
iii) a steady state of permeation is reached when the water flux is constant, and hence the permeability coefficient is determined.

For the G-plasticized nanocomposites, a time-scale shift of water flux curve to lower values is obtained for the G3 nanocomposite indicating a faster water diffusion whereas a shift to higher values is obtained for the G5 nanocomposite reflecting a slower water diffusion. For the G3, the faster diffusion can be related to the hydrophilic character of halloysite nanofiller (surface hydroxyl groups), and for the G5 the reduction of diffusion to the film morphology and the fine dispersion of nanofiller within the starch matrix leading to tortuosity effects. These results are consistent with the previous comments on the permeability variations. For the two other plasticized nanocomposites series, the time-scale shifts of the water flux curves to higher values are obtained indicating a faster water diffusion within the nanocomposites. Then, the weak interfacial interactions and the presence of filler aggregation play the major role and negate the expected tortuosity effects of nanofiller in the films. However, the faster water diffusion in these films is in

good agreement with the permeability changes. This trend can be discussed from water diffusivity, which highlights tortuosity effects in a different way. The water diffusivity values are gathered in Table 2.

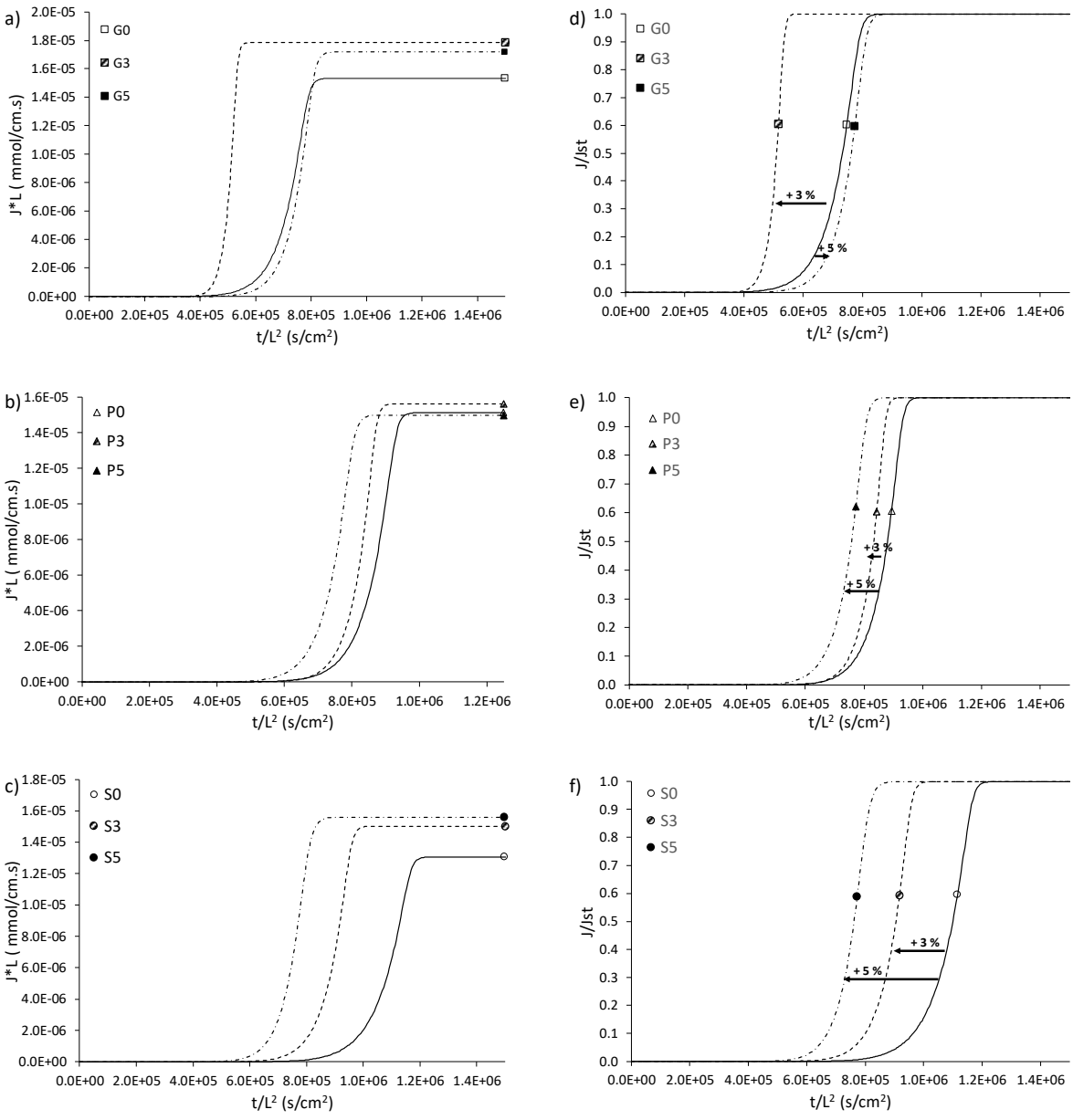

Figure 3. Experimental reduced water flux (a to c) and normalized water flux (d to f) as a function of the reduced time for the different plasticized starch nano-biocomposites.

3.3.2. Water diffusivity vs. filler content.

Sorbed water molecules induce a plasticization phenomenon since water act as a volatile plasticizer. This effect is evidenced by the variations of diffusion coefficients calculated from the slope of the permeation curves by plotting the normalized water flux J/Jst as a function of the reduced time (t/L^2), shown in Figure 3d, e, f. With such a representation, permeation data are analyzed independently of the film thickness. A time-scale shift of the normalized flux curves to lower values is noticeable, reflecting a decrease of the delay time in diffusion, which means that water molecules diffuse more easily. This shift is obtained for all nano-biocomposites, except for G5 nanocomposite. One can state that the quality of interfacial interactions and the filler aggregation, as observed from the SEM observations, has contributed to accelerating the water diffusion mechanism into the starchy films.

Using Fick's law equations assuming that the diffusivity is a constant parameter, the diffusion coefficient can be calculated at two specific times during the transient regime of permeation process, as already described (Marais et al., 2000). Briefly, the coefficient $D_{0.24}$, also called D_I, is determined at the inflexion point t_I corresponding to J/Jst = 0.24 while the coefficient $D_{0.6167}$, also called D_L, is calculated at the time-lag t_L corresponding to J/Jst = 0.6167. In addition, the limit diffusion coefficient, named D_0, is calculated at nil water content, i.e. at the beginning of the permeation process. The diffusion coefficients are summarized in Table 2.

The comparison of $D_{0.24}$ and $D_{0.6167}$ coefficients provides evidence for a water concentration-dependence of the diffusion (Table 2). In fact, it is usually observed an increase of diffusivity with the increase of permeated water concentration into a film: in that case, $D_{0.24} < D_{0.6167}$ ranking is found. This trend is obtained in the present work, attesting that a water plasticization effect occurs in the starch-based films.

	D_0 10^{-8} $cm^2.s^{-1}$	$D_{0.24}$ 10^{-8} $cm^2.s^{-1}$	$D_{0.6167}$ 10^{-8} $cm^2.s^{-1}$	γC_{eq}	γ $cm^3.mmol^{-1}$	C_{eq} $mmol.cm^{-3}$
G0	2.1	12.7	21.1	4.52	0.127	35.9
G3	2.5	16.3	25.0	4.79	0.129	35.0
G5	1.9	12.3	20.3	4.53	0.116	39.1
P0	1.4	10.8	18.2	4.88	0.119	40.8
P3	1.3	12.6	21.5	5.19	0.149	35.8
P5	1.8	12.4	20.8	4.66	0.131	35.8
S0	1.4	9.9	16.7	4.93	0.154	34.5

S3	1.3	10.1	17.0	4.88	0.115	42.6
S5	1.9	11.8	19.6	4.53	0.118	38.7

Table 2. Water permeation parameters for the different plasticized starch nano-biocomposites with different nanofiller contents (0, 3 and 5 wt%) and plasticizer systems (S, P, G). The average variation of coefficients is around 5%.

The evolution of D coefficients as a function of nanofiller content (Table 2) follows that of permeability coefficients (Figure 2). Calculated at the start of permeation measurement, the limit diffusion coefficient D_0 highlights the transfer of the first water molecules into the films. The increase in D_0 globally suggests an increase in water diffusion with the nanofiller content. This increase in D_0 coefficients is faster for the P-based and S-based nanocomposites indicating a faster diffusion mainly in numerous areas free of fillers considering the filler dispersion/aggregation level. In contrast, a reverse effect is obtained for the G-based starch series confirming certain tortuosity effects by the fine filler dispersion, even though the values are rather high and clearly close to that of the unfilled film. The fact that the diffusion coefficients are higher in the case of G-based nanocomposite series could be explained by the high content in hydrophilic hydroxyl groups in G. In addition, the D coefficient evolution is in good accordance with the time-scale shifts of normalized permeation curves for nano-biocomposite films as a function of nanofiller content.

A set of considerations can explain the diffusivity variation for the nano-biocomposites: i) the hydrophilicity of G has induced higher D_0 values, ii) the incorporation of the nanofiller with hydrophilic functions has increased the D_0 value and iii) the quality of interfacial filler/plasticized starch interactions associated with the nanofiller aggregates size have contributed to create free volumes in the vicinity of aggregates, that have increased the D_0 values for the P-based and S-based starch nanocomposite films. Similar evolutions are obtained for $D_{0.24}$ and $D_{0.6167}$ coefficients during the permeation process. This result again testifies to subtle equilibrium between tortuosity effects and free volumes generated into films favoring the water influx.

3.3.3. Water plasticization effect

622 The water plasticization effect is usually described by an exponential law of diffusivity D with
623 the local water concentration C, as shown in Equation 4. This plasticization effect is usually
624 linked to an increase in the free volume within the film and to the affinity of specific sites
625 such as hydrophilic groups. From the fit of permeation curves by using the exponential law
626 (Equation 4), the plasticization factor γC_{eq} (taken at the steady state of the permeation
627 process), the equilibrium water local concentration C_{eq} and the plasticization coefficient γ
628 are determined. The values are gathered in Table 2. The positive values testify to the water
629 concentration-dependence of the diffusion coefficient (Follain et al., 2010). The high values
630 of γC_{eq} close to 5 clearly conform to hydrophilic materials, such as starchy materials, and/or
631 materials showing a high affinity to water. The presence of plasticizer did not alter it. Then,
632 the affinity of hydrophilic groups of plasticized starch to water molecules is clearly evidenced
633 from water permeation measurements. Very few other effects are noted with the increase
634 of nanofiller content, except for the highest content for which the plasticization factor is
635 slightly reduced likely due to the nanofiller dispersion state at this content. The effect on
636 plasticization coefficient γ is too small without marked trends to give an explanation from
637 these values. In addition, few changes in water concentration C_{eq} are noted as the nanofiller
638 content increases, suggesting that the water solubility of starchy matrix is higher than that of
639 nanofiller. This can be likely in accordance with the hydrophilic nature of starch and the high
640 γC_{eq} values as mentioned in Table 2. The lowest values were again obtained with the S-
641 plasticized starch film series, as measured from water permeability coefficients. This finding
642 can be related to the lower water affinity of S compared to G and to the crystallization of S
643 during storage before measurement which can embrittle the corresponding plasticized
644 starch films (Xie et al., 2013).

645 To abstract, although the water plasticization effect is clearly noticed, when observing good
646 nanofiller-starch interfacial interactions in the nanocomposite films, tortuosity effects of the
647 nanofiller play the major role, whereas when observing weak nanofiller-starch interfacial
648 interactions, the expected improvement due to the incorporation of the nanofiller is not
649 found.

650 **3.4. Evolution of water hydration properties**

651 The effects of plasticizer type and of halloysite nanotubes content on water vapor sorption
652 behavior and water vapor diffusivity were investigated. The standard deviation of the

653 average thickness of the film samples is under 5%. The equilibrium water vapor gains,
654 expressed in g/100 g dry basis of polymer film, at each water activity were obtained from the
655 equilibrium state of water sorption kinetic profiles. The resulting water vapor sorption
656 isotherms for the unfilled plasticized starch films and for the three series of nanocomposites
657 films are presented in Figures 4 and 5, respectively. The shape of the sorption isotherms
658 conforms to a Flory-Huggins-type profile, included in the Brunauer-Emmett-Teller
659 classification (Brunauer, Deming, Deming, & Teller, 1940) among the five general types. Such
660 a sorption isotherm shape is typical of water sorption in many hydrophilic and carbohydrate
661 polymer-based films (Labuza, 1968; Enrione et al., 2007; Rocca et al., 2007; Zeppa et al.,
662 2009; Chivrac et al., 2010a; Ayadi & Dole, 2011; Follain et al., 2013; Cheviron et al., 2016).
663 Some authors have found a sigmoidal shape for the isotherm curves for starch plasticized
664 with less than 20 wt% of G (Enrione et al., 2007; Zeppa et al., 2009; Ayadi & Dole, 2011;
665 Follain et al., 2013; Cheviron et al., 2016) and others authors have reported, as in the
666 present work, an exponential increase in water uptake corresponding to type III isotherm in
667 the classification for starch films plasticized with over 20 wt% of G (Rocca et al., 2007;
668 Chivrac et al., 2010a, Ayadi, & Dole, 2011). From the work of Ayadi and Dole (Ayadi, & Dole,
669 2011) on the study of the saturation of sorption sites (mainly OH sites) of starch by G and
670 water (water vapor sorption) using a gravimetric technique, one can explain this difference
671 in sorption profiles. According to this study, saturation concentrations of starch by water
672 molecules and G were found to be of 24 and 22 wt%, respectively, for which the plasticizers
673 are strongly sorbed onto starch preventing the water vapor sorption during sorption
674 measurement, which leads to zero water vapor uptake. From this finding, it seems relevant
675 to obtain none water mass gain at low water activities, as reported in Figures 4 and 5 since
676 the used plasticizer contents (23% wt% of G and 23 wt% of water in the present work) are
677 very close to saturation concentrations found in the previous work (Ayadi, & Dole, 2011). In
678 addition, Enrione et al (Enrione et al., 2007) have intuitively stated that higher G
679 concentration than 20 wt% d.b. reduced the water uptake at low water activities due to
680 strong G-starch hydrogen bonds considered to be as the main force involved in the water
681 sorption mechanism, as already suggested by Myllärinen (Myllärinen et al., 2002). Ayadi and
682 Dole (Ayadi, & Dole, 2011) have also linked their experimental and extrapolated results to
683 stoichiometric and steric considerations, suggesting that the anhydroglucose unit behaves as
684 a monofunctional substrate for G and as a trifunctional substrate for water. Then, ternary

starch-G-water systems can be considered as complex systems where water is in competition with G. Two types of sorption curve profiles were accordingly observed in the literature for starch-based films depending on the plasticizer/starch composition.

Concerning the experimental isotherms profiles (Figures 4 and 5), the first part corresponds to weak/none sorbent/starch interactions occurring at low water activities due to strong plasticizers/starch interactions by hydrogen bonds between hydroxyl groups of plasticizers with functional groups of starch reducing drastically the number of accessible water sorption sites, and the second part conforms to water cluster contribution at higher water activities. Opposite behavior was detected as a function of water activity. At low water activities hydrogen bonds interactions were the main force involved in the sorption mechanism whereas at high water activities water-water interactions became the driving force of sorption mechanism resulting in accelerated uptakes. The water sorption seems also to be easier on the first sorbed water layer than directly on the starchy film surface. The water vapor mass gains for the studied films remained very low below water activity 0.5 and then sharply increased above water activity 0.6 (Figures 4 and 5). This trend is obtained whatever the plasticizer used and the nanofiller content. Values under 60% were measured for water activities up to 0.9, which is in accordance with those reported in previous studies on starch-based materials considering different parameters such as the plasticizer content, the starch origin and the water sorption method (using saturated salt solutions method *vs.* water sorption microbalance *vs.* desorption method) (Mali et al., 2005; Enrione at al., 2007; Zhang et al., 2008; Zeppa et al., 2009; Chivrac et al., 2010a; Ayadi, & Dole, 2011; Cheviron et al., 2016).

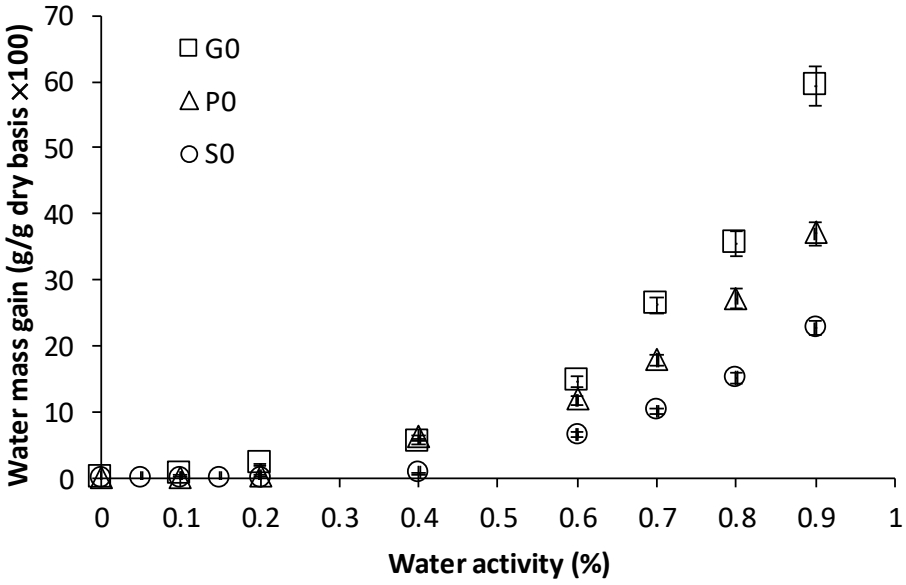

Figure 4. Water vapor sorption isotherms for the unfilled plasticized starch films (vertical bars standing for the standard deviations are too low to be clearly visible on the graph).

Regarding the unfilled plasticized starch films (Figure 4), the water vapor sorption isotherms show identical behavior below water activities 0.3, the amount of specific sorption sites seems to be almost identical and is independent of the plasticizer. This result is related to the strong plasticizer-starch hydrogen bonds which led to an unavailability of specific polar sites in the plasticized films, as above-mentioned. From water activities over 0.4, the water mass gain can be correlated with the hydrophilic character of the plasticizer. The higher hydrophilic character of G has induced the higher water mass gain. The lower water content is obtained for the S-plasticized starch film. This result agrees with previous results (Lourdin et al., 2003; Mali et al., 2005; Chivrac et al., 2010a). This trend is increased for water activities over 0.7, due to the water clustering formation, as classically occurring at these high activities. This result suggests a cumulative effect of plasticizer and starch polar sites interacting with sorbed water molecules, and hence, plasticizers have facilitated water sorption phenomenon. Indeed, at this relatively high plasticizer content, a phase separation is induced, with plasticizer-rich and carbohydrate rich phases, as already claimed (Chivrac et al., 2010a, Ayadi & Dole, 2011), allowing starch polar sites to be more accessible to additional sorbed water molecules. This accessibility is also related to the S/G ratio, i.e. to

728 the higher plasticizing efficiency of G contributing to the higher water uptake. There is
729 accordingly an increase in the molecular mobility by plasticization effect of plasticizers and
730 water, which induced free volumes within the films favoring additional water influx. Again,
731 the S-plasticized starch film is indicated as more water resistant and less hygroscopic than
732 the two others plasticized films, which reduced interactions with water molecules. G-
733 plasticized starch films appeared as less water resistant due to higher hydrophilicity of this
734 plasticizer. Furthermore, the storage-induced S crystallization, as shown by XRD
735 measurements and reported in the literature, is certainly responsible for this higher water
736 resistance.

737 Regarding the filled plasticized starch films (Figure 5), the water vapor sorption isotherms
738 present similar profiles meaning that the sorption mechanism is unmodified in comparison
739 with the reference films. Contrary to the literature concerning filled plasticized starch
740 materials (Zeppa et al., 2009; Chivrac et al., 2010a; Chivrac et al., 2010c; Cheviron et al.,
741 2016) where none logical and regular trends were reported, we have observed in the
742 present work a reduction of water uptake with the nanofiller content increase, more
743 specifically in the high-water activity range. This behavior is found to be dependent on the
744 plasticizer type. This continuous and regular trend is an indication that the nanocomposites
745 are rather less hydrophilic than the references films. Indeed, the experimental values are
746 found to be lower than theoretical values calculated from the additivity law. It seems that
747 the halloysite nanotubes considered as impermeable entities like nanofillers in general and
748 the dispersion quality have positively impacted the water vapor sorption mechanism, even if
749 the reduction cannot be considered significant. In a general point of view, one can state that
750 the incorporation of halloysite nanotubes did not drastically affect the water sorption
751 capacity of the starch matrix.

752

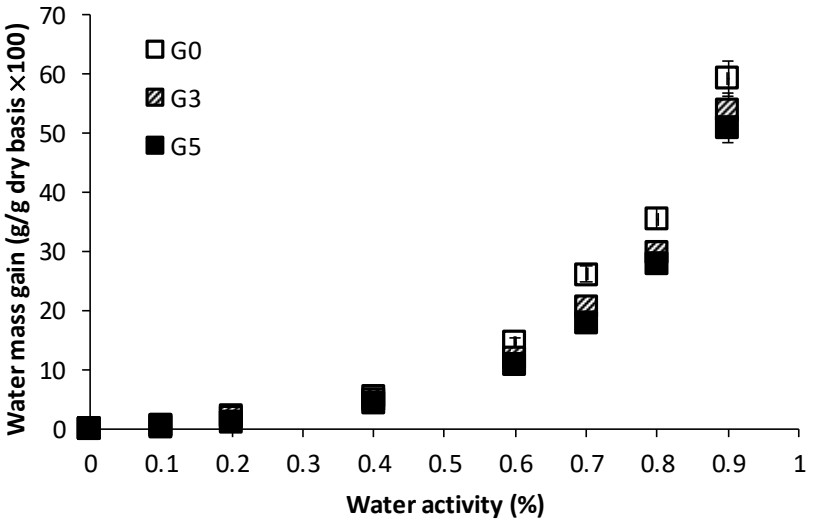
G0
G3
G5
Water mass gain (g/g dry basis ×100)
Water activity (%)
0
10
20
30
40
50
60
70
0
0.1
0.2
0.3
0.4
0.5
0.6
0.7
0.8
0.9
1

753

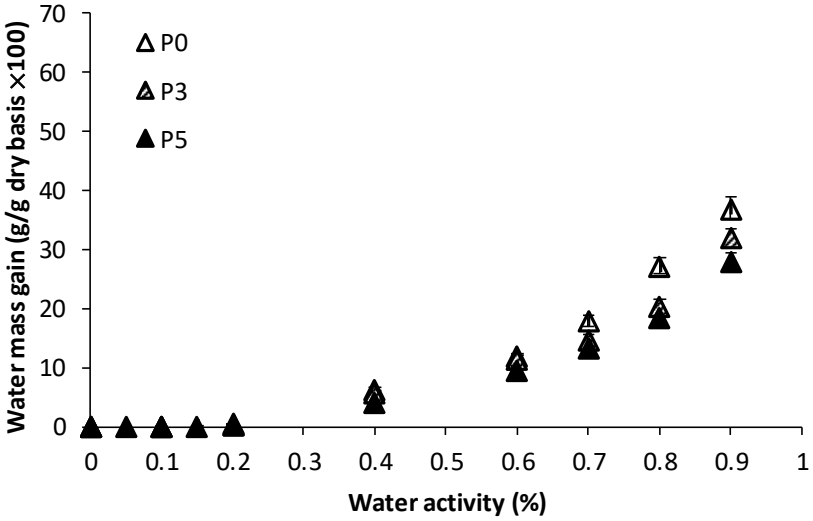
P0
P3
P5
Water mass gain (g/g dry basis ×100)
Water activity (%)
0
10
20
30
40
50
60
70
0
0.1
0.2
0.3
0.4
0.5
0.6
0.7
0.8
0.9
1

754

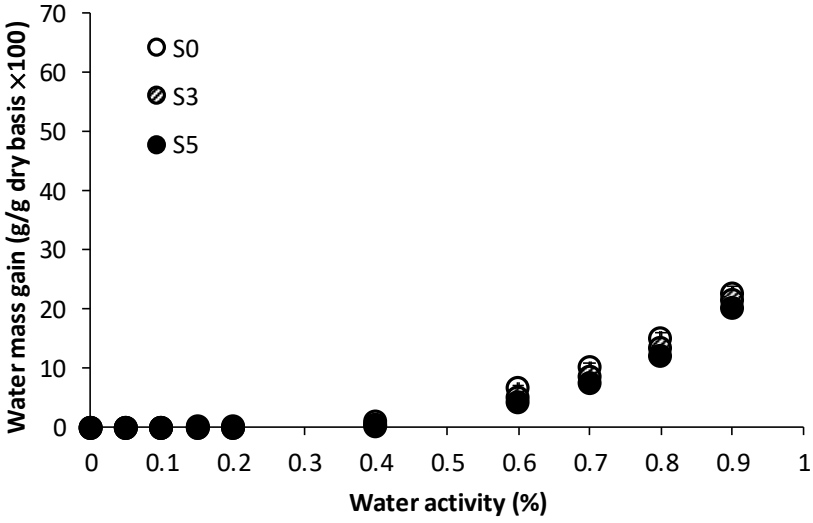
S0
S3
S5
Water mass gain (g/g dry basis ×100)
Water activity (%)
0
10
20
30
40
50
60
70
0
0.1
0.2
0.3
0.4
0.5
0.6
0.7
0.8
0.9
1

755

Figure 5. Water vapor sorption isotherms for the different starch-based nano-biocomposites. (vertical bars standing for the experimental errors are low to be clearly visible on the graph).

The effect of the incorporation of halloysite nanotubes on the water vapor diffusion was also investigated. The water vapor diffusion coefficients as a function of the water mass gain (i.e. water content at sorption equilibrium) in a semi-logarithmic scale are plotted, as represented and exemplified for the G-plasticized starch films in Figure 6 (for a better reading of D variations). Similar evolutions are obtained for the two other nanocomposite series. The D coefficient is not constant and its evolution is found to be dependent on the amount of water molecules sorbed by the films. Irrespective of the films, three distinct domains are clearly observed. The diffusion coefficients decreased rapidly and then increased to decrease again at the highest water mass gains. Such changes in diffusion coefficients with the amount of water molecules sorbed are generally shown in the literature (Marzec, & Lewicki, 2006; Enrione et al., 2007; Belbekhouche et al., 2011; Chivrac et al., 2010a; Masclaux et al., 2010; Follain et al., 2010; Cheviron et al., 2015) and are typical of water sorption in many hydrophilic and carbohydrate polymer-based films. However, one can mention that the first decrease in D coefficient at low sorbed water concentration is not always reported owing to the choice of the wide range of water activities applied. The changes in diffusion coefficients agree well with the water vapor sorption mechanism complying with the shape of Flory-Huggins-type profile sorption curves.

The first decrease of D coefficient at low water mass gains can be explained by an antiplasticizing effect of water molecules on diffusion, as previously reported (Gaudin et al., 1999; Merzec, & Lewicki, 2006), which usually takes place at low sorbed water concentrations. A strong cohesion was established between water and plasticizer starch film, which has reduced the water mobility. The increase of D coefficient is due to the typical plasticizing effect of water which has favored the starch chains mobility and then the diffusion of water molecules within the film. Water molecules were preferentially dissolved in free volumes of material and sorbed on the specific sorption sites of the film components which became accessible by plasticization. For the highest water mass gains, the decrease of D coefficient is related to the water clustering formation which makes water molecules less mobile (Barrie, & Platt, 1963), in particular with the increase of the water cluster size.

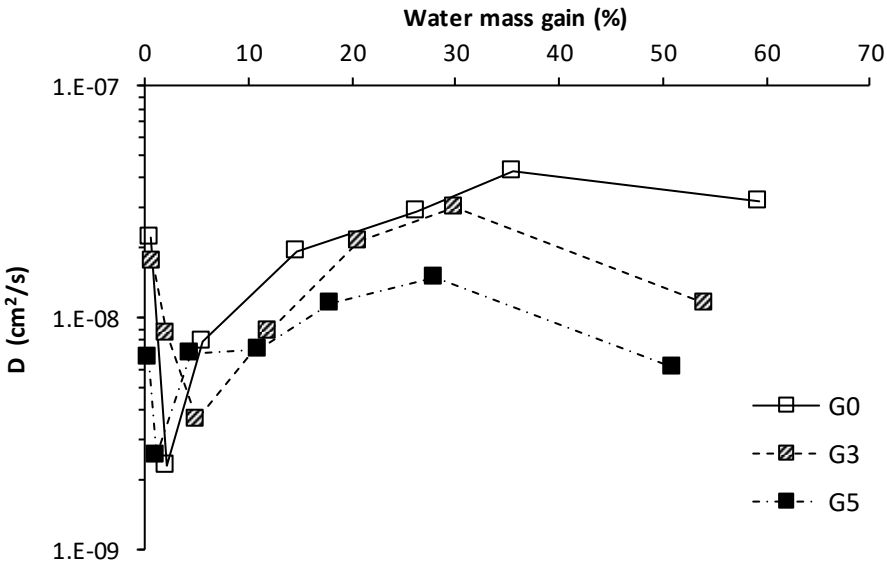

Figure 6. Water vapor diffusion coefficient versus water activity for the G-plasticized starch nano-biocomposites. The average standard deviations are equal to 5%.

Concerning the effect of the nanofiller addition, as shown in Figure 6, the shape of the curve is similar to that of the unfilled starch film. Increasing the halloysite nanotubes content led to decrease the water diffusion coefficient. This difference can be explained by the presence of crystalline halloysite nanotubes considered as obstacles for water diffusion, which were able to limit in a higher extent the diffusion of water molecules in the starchy matrix. Even at these low contents, the tortuosity effect brought by the nanofiller within the plasticized starch matrix has also helped to decrease the water diffusion, as observed from water permeation measurements. A similar trend is obtained for the two others nanocomposites series but in a lesser extent since the reduction of water diffusion coefficient is weaker. On one hand, the quality of nanofiller-matrix interfaces has likely played a role into the limitation of the water diffusion for the G-plasticized starch film, and in a lesser extent for the films plasticized with S since presenting a weaker adhesion. On the other hand, one can consider the impact of the G/S ratio on the water diffusion phenomenon. At high G content, the hydrophilic character and the plasticizing ability of G have thus facilitated the water supply in the film.

4. Conclusion

Nano-biocomposites based on potato starch containing halloysite nanotubes as nanofiller and G, P mixture and S as plasticizers were successfully prepared to obtain 200 µm multiphase films. As a function of plasticizer type used and the halloysite nanotubes content, the films exhibited differences in their morphology and microstructure. In presence of the nanofiller, good filler-matrix interfacial interactions without filler aggregates was observed for the G-plasticized starch films while weak interactions were observed for P- and S-plasticized starch films with some filler aggregates.

The water uptake is correlated to the plasticizing efficiency of the plasticizers. We can also observe the cumulative effect of plasticizers and starch polar sites. With filler, a reduction of water uptake was shown, more specifically for high water activity. The nano-biocomposites became accordingly less hydrophilic than the unfilled systems without affecting the sorption capacity of starch. Increasing the filler content has led to a decrease of the water diffusivity due to the crystalline and inorganic nature and tortuosity effects of the halloysite nanotubes. When adding halloysite nanotubes, the water permeability increased due to its water affinity. When the filler content increases, a reduction of permeability is measured for the films presenting good interfacial interactions and tortuosity effects by fine nanotubes dispersion. The water plasticization effect was evidenced by time-scale shift of permeation curves indicating that water molecules diffuse more easily in bio-nanocomposites. The reverse effect for G5 film confirmed tortuosity effects resulting from the high filler dispersion and good filler-starch interfacial interactions. The tortuosity effects were thus highlighted and this trend was exacerbated by the quality of filler-starch interfacial interactions and filler dispersion.

Based on these results, glycerol could be a good candidate to ensure optimized filler-starch interfacial interactions combined with a fine nanofiller dispersion. Such nano-biocomposites systems could find different applications for short-term applications, such as packaging films or agricultural mulch films where such characteristics in water/gas transfer are often required.

References

Alexandre, M., & Dubois. P. (2000). Polymer-layered silicate nanocomposites: preparation, properties and uses of a new class of materials. Materials Science and Engineering R-reports, 28(1), 1-63.

Anglès, M.N., Dufresne, A. (2000). Plasticized starch/tunicin whiskers nanocomposites. 1. Structural analysis. *Macromolecules*, 33, 8344-8353.

Avérous, L. (2004). Biodegradable multiphase systems based on plasticized starch: A review. *Journal of Macromolecular Science-Polymer Reviews*, C44(3), 231-274.

Avérous, L., & Pollet, E. (2012). Green nano-biocomposites. In Environmental silicate nano-biocomposites; Avérous, L., Pollet, E., Eds.; Springer: London, UK, ISBN 978-1-4471-4101-3, 1-11.

Ayadi, F., & Dole, P. (2011). Stoichiometric interpretation of thermoplastic starch water sorption and relation to mechanical behavior. *Carbohydrate Polymers*, 84, 872-880.

Baker, R.W., & Wijmans, J.-G. (1994). Polymeric gas separation membranes, CRC Press, Boca Raton.

Barrie, J.A., & Platt, B. (1963). The diffusion and clustering of water vapour in polymers, *Polymer,* 4, 303–313.

Belbekhouche, S., Bras, J., Siqueira, G., Chappey, C., Lebrun, L., Khelifi, B., Marais, S., & Dufresne, A. (2011). Water sorption behavior and gas barrier properties of cellulose whiskers and microfibrils films. *Carbohydrate Polymers*, 83, 1740–1748.

Bertolino, V.; Cavallaro, G.; Milioto, S.; Lazzara, G. (2020). Polysaccharides/Halloysite nanotubes for smart bionanocomposite materials. *Carbohydrate Polymers*, 245, 116502

Bharadwaj, R.K. (2001). Modeling the barrier properties of polymer-layered silicate nanocomposites. *Macromolecules*. 34(26), 9189-9192

Brunauer, S., Deming, L.S., Deming, W.E., Teller, E. (1940). On a theory of the van der Waals adsorption of gases. *Journal of the American Chemical Society*, 62(7), 1723-1732.

Cheviron, P., Gouanvé, F., & Espuche, E. (2015). Starch/silver nanocomposite: effect of thermal treatment temperature on the morphology, oxygen and water transport properties. *Carbohydrate Polymers*, 134, 635-645].

Cheviron, P., Gouanvé, F., & Espuche, E. (2016). Preparation, characterization and barrier properties of silver/montmorillonite/starch nanocomposite films. *Journal of Membrane Science*, 497, 162-171

Chivrac, F., Angellier-Coussy, H., Guillard, V., Pollet, E., Avérous, L. (2010a) "How does water diffuse in starch/montmorillonite nano-biocomposite materials?" *Carbohydrate Polymers*. 82/1, 128–135.

Chivrac, F., Pollet, E., Schmutz, M., Avérous, L. (2010b). Starch nano-biocomposites based on needle-like sepiolite clays. *Carbohydrate Polymer*s, 80, 145-153.

Chivrac, F., Pollet, E., Dole, P., Avérous, L. (2010c). Starch-based nano-composites: plasticizer impact on the montmorillonite exfoliation process. *Carbohydrate Polymers*, 79, 941-947.

Crank, J. (1967). The mathematics of diffusion, Clarendon Press, Oxford.

Enrione, J. I., Hill, S. E., Mitchell, J.R. (2007) Sorption behavior of mixtures of glycerol and starch. Journal of Agricultural and Food Chemistry. 55(8), 2956-2963.

Follain, N., Valleton, J-M., Lebrun, L., Alexandre, B., Schaetzel, P., Metayer, M., & Marais, S. (2010) Simulation of kinetic curves in mass transfer phenomena for a concentration-dependent diffusion coefficient in polymer membranes, *Journal of Membrane Science*., 349, 195-207.

Follain, N., Belbekhouche, S., Bras, J., Siqueira, G., Marais, S., & Dufresne. A. (2013). Water transport properties of bio-nanocomposites reinforced by Luffa cylindrica cellulose nanocrystals. *Journal of Membrane Science*, 427, 218-229.

Follain, N., Alexandre, B., Chappey, C., Colasse, L., Médéric, P., & Marais, S. (2016) Barrier properties of polyamide 12/montmorillonite nanocomposites: Effect of clay structure and mixing conditions. *Composites Science and Technology*, 136, 18-28.

Gaudin, S., Lourdin, D., Forssell, P.M., & Colonna, P. (2000). Antiplasticisation and oxygen permeability of starch-sorbitol films. *Carbohydrate Polymers*, 43, 33-37.

Gaudin, S., Lourdin, D., Le Botlan, D., Ilari, J. L., & Colonna, P. (1999). Plasticisation and mobility in starch–sorbitol films. *Journal of Cereal Science*, 29(3), 273–284.

Gorrasi, G., Tortora, M., Vittoria., Pollet, E., Lepoittevin, B., Alexandre, M., Dubois, P. (2003). Vapor barrier properties of polycaprolactone montmorillonite nanocomposites : effect of clay dispersion. *Polymer*, 44(8), 2271-2279.

He, Y.; Kong, W.; Wang, W.; Liu, T.; Liu, Y.; Gong, Q.; Gao, J. (2012). Modified natural halloysite/potato starch composite films. *Carbohydrate Polymers*, 87, 2706-2711.

Labuza, T.P. (1968). Sorption phenomena in foods*. Food Technology*, 22, 15-24.

Liu, M., Guo, B., Du, M., Chen, F., Jia, D. (2009). Halloysite nanotubes as a novel β-nucleating agent for isotactic polypropylene. *Polymer*, 50, 3022-3030.

Lourdin, D., Coignard, L., Bizot, H., & Colonna, P. (1997). Influence of equilibrium relative humidity and plasticizer concentration on the water content and glass transition of starch materials. Polymer, 38(21), 5401–5406.

Lourdin, D., Colonna, P., Ring, S.G. (2003). Volumetric behaviour of maltose-water, maltose-glycerol and starch-sorbitol-water systems mixtures in relation to structural relaxation. *Carbohydrate Research*, 338(24), 2883-2887.

Makaremi, M., Pasbakhsh, P., Cavallaro, G., Lazzara, G., Aw, Y. K., Lee, S. M., & Milioto, S. (2017). Effect of morphology and size of halloysite nanotubes on functional pectin bionanocomposites for food packaging applications. *ACS Applied Material and Interfaces*, 9, 17476-01488.

Mali, S., Sakanaka, L.S., Yamashita, F., Grossmann, M.V.E. (2005). Water sorption and mechanical properties o cassava starch films and their relation to plasticizing effect, *Carbohydrate Polymers*, 60, 283-289.

Marais, S., Metayer, M., &Labbe, M. (1999) Water diffusion and permeability in unsaturated polyester resin films characterized by measurements performed with a water-specific permeameter: analysis of the transient permeation, *Journal of Applied Polymer Science,* 74, 3380-3395.

Marais, S., Nguyen, Q.T., Devallencourt, C., Metayer, M., Nguyen, Q.T.U., & Schaetzel, P. (2000) Permeation of water through polar and nonpolar polymers and copolymers: determination of the concentration-dependent diffusion coefficient, *Journal of Polymer Science part B: Polymer Physics.*, 38, 1998-2008.

Marzec, A., & Lewicki, P. P. (2006). Antiplasticization of cereal-based products by water. Part I. Extruded flat bread. *Journal of Food Engineering*, 73, 1–8.

Masclaux, C., Gouanvé, F., & Espuche, E. (2010). Experimental and modelling studies of transport in starch nanocomposite films as affected by relative humidity. *Journal of Membrane Science*, 363(1–2), 221–231.

Métayer, M., Labbé, M., Marais, S., Langevin, D., Chappey, C., Dreux, F., Brainville, M., & Belliard, P. (1999). Diffusion of water through various polymer films: a new high performance method of characterization. *Polymer Testing*, 18, 533-549.

Myllärinen, P., Partanen, R., Jukka, S., Forssell, P. (2002). Effect of glycerol on behaviour of amylose and amylopectine films. *Carbohydrate Polymers*, 50, 355-361.

Nechyporchuk, O.; Belgacem, M.N.; Bras, J. (2016). Production of cellulose nanofibrils: A review of recent advances. *Ind. Crop. Prod*., 93, 2–25.

Pasbakhsh, P.; De Silva, R.; Vahedi, V.; Jock Churchman, G. (2018). Halloysite nanotubes: Prospects and challenges of their use as additives and carriers -A focused review. *Clay Min*., 51, 479–487.

Prager, S., & Long, F.A. (1951). Diffusion of Hydrocarbons in Polyisobutylene*. Journal of the American Chemical Society*, 73, 4072-4075.

Ren, J., Dang, K. M., Pollet, E., & Averous, L. (2018). Preparation and characterization of thermoplastic potato starch/halloysite nano-biocomposites: effect of plasticizer nature and nanoclay content., *Polymers*, 10, 808-822.

Rindlav-Westling, A., Stading, M., Hermansson, A.M., Gatenholm, P. (1998). Structure, mechanical and barrier properties of amylose and amylpectin films. *Carbohydrate Polymers*, 36(2-3), 217-224.

945 Robeson, L.M. (2008). The upper bound revisited. *Journal of Membrane Science*, 320, 390-
946 400.

947 Rocca, E., Broyart, B., Guillard, V., Guilbert, S., Gontard, N. (2007). Controlling moisture
948 transport in a cereal porous product by modification of structural or formulation
949 parameters. *Food Research International*, 40, 461-469.

950 Schmitt, H., Prashantha, K., Soulestin, J., Lacrampe, M.F., & Krawczak, P. (2012). Preparation
951 and properties of halloysite nanotubes/plasticized Dioscorea opposite Thunb. Starch
952 composites. *Carbohydrate Polymers*, 89, 920-927.

953 Swanson, C. L., Shogren, R. L., Fanta, G. F., & Imam, S. H. (1993). Starch-plastic materials –
954 Preparation, physical properties, and biodegradability (a review of recent USDA research).
955 *Journal of Environmental Polymer Degradation*, 1(2), 155-166.

956 Tang, X., Alavi, S., Herald, T. (2008). Effects of plasticizers on the structure and properties of
957 starch-clay nanocomposite films. *Carbohydrate Polymers*, 74(3), 552-558.

958 Talja, R.A., Helén, H., Roos, Y.H., Jouppila, K. (2007). Effect of various polyols and polyol
959 contents on physical and mechanical properties of potato starch-based films. *Carbohydrate*
960 *Polymers*, 67, 288-295.

961 Tang, X-G, Hou, M., Zou, J., Truss, R. (2013). Poly(vinylidene fluoride)/halloysite nanotubes
962 nanocomposites: the structures, properties, and tensile fracture behaviors. *Journal of*
963 *Applied Polymer Science*, 128, 869-878.

964 Van Krevelen, D. W. (1997). *Properties of polymers*, 3rd ed., Elsevier Sciences: The
965 Netherlands, **1997**.

966 Van Soest, J., Hulleman, S., De Wit, D., Vliegenthart, J. (1996a). Crystallinity in starch
967 bioplastics. *Industrial Crops and Products*, 5/1, 11-22.

968 Van Soest J., Hulleman S., De Wit D., Vliegenthart, J.F.G. (1996b). Changes in mechanical
969 properties of thermoplastic potato starch in relation with changes in B-type crystallinity.
970 *Carbohydrate Polymers*, 29/3, 225-232.

971 Wang, Q.; Ju, J.P.; Tan, Y.Q.; Hao, L.Y.; Ma, Y.L.; Wu, Y.; Zhang, H.W.; Xia, Y.Z.; Sui, K.Y.
972 (2019). Controlled synthesis of sodium alginate electrospun nanofiber membranes for multi-

973 occasion adsorption and separation of methylene blue. *Carbohydrate Polymers*, 205, 125–
974 134.

975 Wu, Y. ; Zhang, Y. ; Ju, J. ; Yan, H.; Huang, X.; Tan, Y. (2019). Advances in halloysite
976 nanotubes-polysaccharide nanocomposite preparation and applications. *Polymers*, 11, 987.

977 Xie, Y., Chang, P.R., Wang, S., Yu, J., Ma, X. (2011). Preparation and properties of halloysite
978 nanotubes/plasticized Dioscorea opposite Thun. Starch composites. *Carbohydrate Polymers*,
979 83, 186-191.

980 Xie, F., Pollet, E., Halley, P.J., & Avérous, L. (2013). Starch-based nano-biocomposites.
981 *Progress in Polymer Science*, 38, 1590-1628

982 Zeppa, C., Gouanvé, F., Espuche, E. (2009). Effect of a plasticizer on the structure of
983 biodegradable starch/clay nanocomposites: thermal, water-sorption, and oxygen-barrier
984 properties. *Journal of Applied Polymer Science*, 112, 2044-2056.

985 Zhang, Y., Han, J.H. (2008). Sorption isotherm and plasticization effect of moisture and
986 plasticizers in pea starch film. *Journal of Food Science*, 73, 313-324.

987